

RSC Advances



This is an *Accepted Manuscript*, which has been through the Royal Society of Chemistry peer review process and has been accepted for publication.

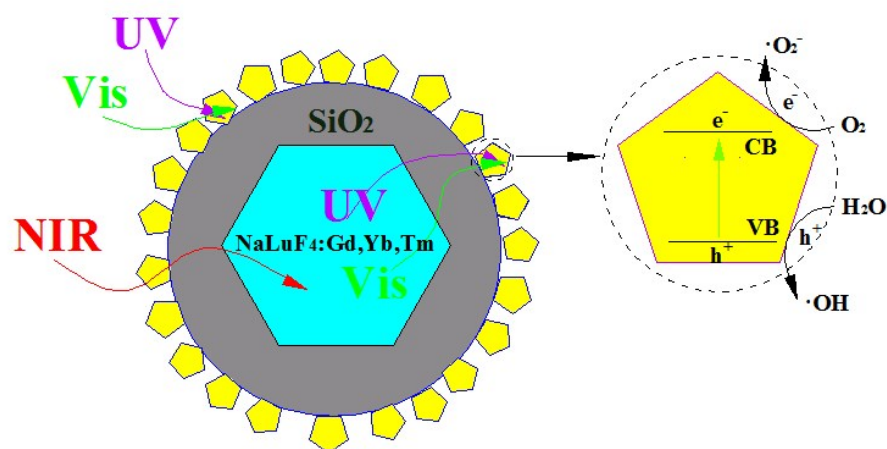
Accepted Manuscripts are published online shortly after acceptance, before technical editing, formatting and proof reading. Using this free service, authors can make their results available to the community, in citable form, before we publish the edited article. This *Accepted Manuscript* will be replaced by the edited, formatted and paginated article as soon as this is available.

You can find more information about *Accepted Manuscripts* in the [Information for Authors](#).

Please note that technical editing may introduce minor changes to the text and/or graphics, which may alter content. The journal's standard [Terms & Conditions](#) and the [Ethical guidelines](#) still apply. In no event shall the Royal Society of Chemistry be held responsible for any errors or omissions in this *Accepted Manuscript* or any consequences arising from the use of any information it contains.

Improving photocatalytic activity by combining with upconversion
nanocrystals and Mo-doping: A case study on β -NaLuF₄:
Gd,Yb,Tm@SiO₂@TiO₂:Mo

Dongguang Yin*, Lu Zhang, Xianzhang Cao, Jingxiu Tang, Wenfeng Huang, Yanlin
Han, Yumin Liu, Tingting Zhang, Minghong Wu*



Improving photocatalytic activity by combining with upconversion nanocrystals and Mo-doping: A case study on β -NaLuF₄: Gd, Yb, Tm@SiO₂@TiO₂:Mo

Dongguang Yin*, Lu Zhang, Xianzhang Cao, Jingxiu Tang, Wenfeng Huang, Yanlin Han, Yumin Liu, Tingting Zhang, Minghong Wu*

School of Environmental and Chemical Engineering, Shanghai University, Shanghai 200444, China

Abstract: A novel double-shell-structured β -NaLuF₄: Gd, Yb, Tm@SiO₂@TiO₂:Mo nanocomposite photocatalyst has been developed for the first time. The nanocomposite consists of uniform β -NaLuF₄: Gd, Yb, Tm upconversion nanocrystals as core, a media shell of SiO₂, and a lot of small sized anatase TiO₂ nanoparticles as the outer shell. The TiO₂ shell is modified by Mo-doping, which can narrow the band-gap of TiO₂ and act as electron traps resulting in enhancement of light absorption and reduction of recombination rate of the photogenerated carriers. The upconversion nanocrystals can convert NIR into UV and visible lights which are overall absorbed by the modified TiO₂ shell. Photocatalytic activities of the prepared products are evaluated through photocatalytic degradation of RhB under the irradiations of simulated solar and NIR lights. The results show that the as-prepared nanocomposite displays a high photocatalytic activity which is significant higher than that of commercial P25 and pure TiO₂. This work provides new insights into the fabrication of TiO₂-based composites as high performance photocatalysts and facilitate their application in environmental protection issues using solar light.

1. Introduction

In recent years, environmental pollution has become a serious problem. Photocatalysis appears as

an effective and environmental friendly technique for the degradation of toxic organic pollutants in air and water.¹⁻³ Most important, clean, safe and renewable solar energy can be used to fulfill this purpose.^{4,5} TiO₂ is considered to be a promising photocatalyst and has been widely used for treating the environmental pollution for its safety, low cost, chemical stability and high photocatalytic activity.⁶⁻¹⁰ However, because of its wide energy band-gap ($E_{bg} \geq 3.2\text{eV}$) and the recombination of photoinduced electron-hole pairs,^{11,12} the practical application of TiO₂ is still limited. Especially, for the utilization of solar light the TiO₂ is ordinarily impuissant, since the ultraviolet light only accounts for a small portion of solar (~5%), which is much lower than that of visible light (~49%) and near-infrared (NIR) light (~46%).^{13,14} As a result, large scale practical application of TiO₂-based photocatalysts to solve environmental and energy problems needs further innovational work.

Up to date, many methods have been adopted to extend the absorption of TiO₂ into the visible light region, e.g. doping of metallic and nonmetallic elements,¹⁵⁻²¹ depositing noble metals,²² coupling with narrow band-gap semiconductors.²³ It is true that the light responsive range can be extended to the long wavelength region (mostly visible light region) with the help of these strategies. However, efficient NIR absorption for photocatalysis is still unreached yet. Especially, the overall catalytic efficiency was not substantially improved. Potential reasons might be that the energy of electron-hole pairs generated by the excitation of long wavelength light are too low to catalyze the reaction and decompose the organic pollutants completely.^{13,14,24} Only those electron-hole pairs produced by the excitation of high energy photons such as UV and near-UV, possess enough high energy to degrade organic pollutants efficiently.^{25,26}

In recently years, some studies including ours have revealed that the construction of

upconversion nanocrystals (UCNCs) and TiO₂ nanocomposites is a potent strategy to improve NIR light harvesting efficiency and photocatalytic activity of TiO₂.²⁷⁻²⁹ The UCNCs can transform NIR to UV and visible lights, which can be absorbed by TiO₂ or modified TiO₂.^{25,30} This approach can not only extend the light responsive range of TiO₂ into the NIR or visible lights regions, but also excite the TiO₂ by high energy photons supplied from the UCNCs. Thus it can substantially improve the photocatalytic efficiency of TiO₂.

In this work, we designed a novel UCNCs-TiO₂ based composite photocatalyst. It is a core-shell structure with double-shell, consisting of β -NaLuF₄:Gd,Yb,Tm (β -UCNCs) as the core, amorphous SiO₂ as the media shell, and UV-vis responsive anatase TiO₂ nanocrystals modified with Mo-doping as the outer shell. It is well-known that NaLuF₄ is a good host material, Yb and Tm ions are the typical sensitive and active ions for upconversion luminescence, and Gd³⁺ doping can promote the transformation of the UCNCs from the cubic to the hexagonal phase resulting in enhancing upconversion luminescence (UCL).^{31,32} Mo⁶⁺, as a transition metal ion, has been used to dope TiO₂ for photocatalytic applications, showing the effects to make the materials catalytically active under visible light.³³⁻³⁵ Based on these, we prepared the β -NaLuF₄:Gd,Yb,Tm as the upconversion nanocrystal firstly and fabricate composite photocatalyst β -UCNCs@SiO₂@TiO₂:Mo (β -UCNCs@SiO₂@TiO₂:Mo) for the study of photocatalytic degradation. The designed structure is different from UCNCs@TiO₂ and UCNCs@SiO₂@TiO₂ core/shell nanostructures reported in previous literatures.^{27-30,36} Based on the designed structure, the upconversion nanocrystals and Mo ions have a synergistic effect which can improve the photocatalytic activity of TiO₂ significantly. The Mo-doping plays a very important role which can narrow the band-gap of TiO₂ and act as electron traps resulting in enhancement of light absorption

and reduction of recombination rate of the photogenerated electron-hole pairs. The as-prepared composite photocatalyst presented a high performance for Rhodamine B (RhB) degradation under the simulated solar light. This work will give a new insight to fabricate of TiO₂-based nanocomposite photocatalysts with high photocatalytic activity under solar and NIR irradiations.

2. Experimental

2.1. Materials

Rare earth oxides Lu₂O₃ (99.999%), Yb₂O₃ (99.999%), Gd₂O₃ (99.999%) and Er₂O₃ (99.999%) were purchased from Shanghai Yuelong New Materials Co. Ltd. Oleic acid (OA) (>90%), 1-octadecene (>90%) and hydroxy propyl cellulose (HPC) were purchased from Sigma-Aldrich. Titanium (IV) ethoxide (>98%), trifluoroacetic acid, RhB, ethanol, tetraethoxysilane (TEOS), sodium carbonate (Na₂CO₃), ammonium hydroxide, ammonium heptamolybdate and cyclohexane were purchased from Sinopharm Chemical Reagent Co., Ltd. (Shanghai). P25 (TiO₂, 99.5%) was purchased from Degussa Co. Ltd. (Germany). Ln(CFCOO)₃ (Ln: Lu, Yb, Gd, Tm) precursors were prepared by dissolving the corresponding metal oxides in trifluoroacetic acid at elevated temperature. All other reagents were analytical grade and were used directly without further purification.

2.2. Synthesis of β -UCNCs

The β -UCNCs was prepared as our previous report with some modification.³⁶ In typically, 10 ml each of the coordinating oleic acid (90%) ligand and the non-coordinating solvent 1-octadecene (90%) were added to the reaction vessel (Solution A). Subsequently, 2 mmol sodium trifluoroacetic

acid (98%) and 1 mmol lanthanide trifluoroacetate precursors were added to the solution containing 5 ml oleic acid and 5 ml 1-octadecene (Solution B). Both A and B solutions were heated to 120° C under vacuum with magnetic stirring and kept for 30 min. Then the solution A was heated to 310°C under N₂ gas atmosphere. After that, the solution B was added to the reaction vessel drop by drop at a rate of 1.5 ml/min. The mixture solution was maintained at this temperature and stirred vigorously for 60 min, then cooled down to 80°C. The formed nanocrystals were precipitated from the solution with addition of excess of ethanol, and collected after centrifuging and washing with hexane/ethanol (1:1 v/v) for three times.

2.3. Synthesis of β -UCNCs@SiO₂ nanoparticles

First, 6.7 mL of octanol and 12 mL of Triton X-100 were dispersed in 50 mL of cyclohexane by sonication and stirring. Then, 5 mL of (0.1 mmol/mL) β -UCNCs cyclohexane solution was added into the above mixture. The resultant solution was stirred for 15 min, and then 0.4 mL of (28 wt%) ammonium hydroxide solution was added to form a reverse microemulsion solution. After stirring for 30 min, 0.3 mL of TEOS was added, and the resultant reaction was aged for 24 h under stirring. The final products (β -UCNCs @SiO₂ nanoparticles) were collected by centrifuging and washed by water and ethanol several times.

2.4. Synthesis of β -UCNCs@SiO₂@TiO₂ nanocomposite

β -UCNCs@ SiO₂ (0.5 mmol) was dispersed in 20 mL of alcohol by sonication treatment. Then, 0.1 g of hydroxypropyl cellulose and 0.1 mL of deionized water were added into the suspension, followed by magnetic stirring for 2 h at room temperature to ensure the sufficient adsorption of hydroxypropyl cellulose by β -UCNCs@ SiO₂. One milliliter of tetrabutyl titanate was added into 5

mL of alcohol to form a transparent solution which was then added into the suspension drop by drop with a speed of 0.5 mL/min. After that, the temperature was increased to 85° C under refluxing conditions for 100 min. The precipitate was isolated by centrifugation, washed with ethanol, and dispersed in 33mL of ethanol to give a β -UCNCs@SiO₂@amorphous TiO₂ suspension. The resulting suspension was transferred to a dried Teflon-lined stainless steel autoclave and heated at 180° C for 24 h in an electric oven. After the reaction, the product was collected by centrifugation and washed with deionized water and ethanol for three times, and then dried at 60 °C in a vacuum oven.

For preparation of β -UCNCs-TiO₂ physical mixture, the β -UCNCs and TiO₂ were synthesized according to the above procedure first, then they were mixed mechanically in the same ratio of β -UCNCs and TiO₂ as that of the β -UCNCs @ SiO₂@ TiO₂ nanocomposite.

2.5. Synthesis of β -UCNCs@ SiO₂@TiO₂:Mo nanocomposite

The as-obtained β -UCNCs@SiO₂@amorphous TiO₂ suspension was mixed with 17 mL of deionized water containing 0.259 g of (NH₄)₆Mo₇O₂₄.4H₂O by sonication and magnetic stirring for 30 min. The resulting suspension was transferred to a dried Teflon-lined stainless steel autoclave and heated at 180° C for 24 h in an electric oven. After the reaction, the final product was collected by centrifugation and washed with deionized water and ethanol for three times, and then dried at 60 °C in a vacuum oven.

2.6. Characterizations

The sizes and morphologies of prepared products were characterized with a JEOL JEM-2010F

transmission electron microscope (TEM) operating at 200 kV. Energy-dispersive X-ray analysis (EDX) of the samples was performed during high-resolution transmission electron microscopy (HRTEM) measurements to determine the elements of the samples. The crystal phase structures of the as-prepared samples were examined by powder X-ray diffraction (XRD) measurements that were performed on a Rigaku D/max-2500 X-ray diffractometer using Cu K α radiation. The scan was performed in the 2θ range from 10° to 80° with a scanning rate of $8^\circ/\text{min}$. The upconversion luminescence spectra were recorded with an Edinburgh FLS-920 fluorescence spectrophotometer using an external 0-2 W adjustable laser (980 nm, Beijing Hi-Tech Optoelectronic Co., China) as the excitation source instead of the Xenon source in the spectrophotometer. UV-vis absorption spectra were measured on a Hitachi 3010 UV-vis spectrophotometer (Japan). All the photoluminescence studies were carried out at room temperature.

2.7. Photocatalytic experiments

Photocatalysis was performed via monitoring RhB degradation by measuring the variation of optical absorption of RhB with a Hitachi U-3010 spectrophotometer, using SGY-IB multifunction of photochemical reactor (Nanjing Sidongke Electric Co. Ltd.) as photocatalytic reaction device. In a typical experiment, 20 mg of sample (catalyst) was dispersed into a quartz cuvette containing 50 mL of RhB aqueous solution (20 mg/L). The suspension was magnetically stirred in the dark for 30 min to attain adsorption-desorption equilibrium between dye and catalyst. Then the photoreaction vessels were exposed to the simulated solar light irradiation produced by a 500 W Xe lamp (PL-X500D) (wavelength distribution: 300-2500nm). At giving time intervals, the photoreacted solutions were analyzed by recording variations of the absorption band maximum (554 nm) in the

UV-Visible spectra of RhB.

The degradation ratio η (%) of dye was calculated using the following equation:

$$\begin{aligned}\eta (\%) &= [(C_0 - C) / C_0] \times 100 \\ &= [(A_0 - A) / A_0] \times 100\end{aligned}$$

Where C_0 and C are the initial and residual concentrations of RhB in solution respectively, and A_0 and A are the absorbance of RhB at 554nm before and after exposing under simulated solar light respectively.

3. Results and discussion

3.1. Phase and morphology characterization

Fig. 1 shows the XRD patterns of the as-prepared products of β -UCNCs, β -UCNCs@SiO₂@TiO₂ and β -UCNCs@SiO₂@TiO₂:Mo. Major XRD peaks of the three samples can be indexed to β -NaLuF₄ (JCPDS No. 27-0726).³⁸ As shown in the XRD patterns of β -UCNCs@SiO₂@TiO₂ and β -UCNCs@SiO₂@TiO₂:Mo nanocomposites (Fig. 1b and 1c), the characteristic diffraction peaks of TiO₂ are observed which are assigned to anatase titania according to the JCPDS No. 21-1272,³⁹ confirming the formation of layer of anatase TiO₂. No impurity peaks can be identified from the XRD pattern, indicating the desired products are synthesized successfully. Due to the coating with SiO₂ and TiO₂ layers, the relative diffraction intensity of β -UCNCs in β -UCNCs@SiO₂@TiO₂ and β -UCNCs@SiO₂@TiO₂:Mo were slightly weakened compared to that of pure β -UCNCs.⁴⁰

The TEM images of prepared products are shown in Fig. 2. As shown in Fig. 2a, NaLuF₄: Gd, Yb, Tm nanocrystals are hexagonal structure with average diameter of about 45 nm. The morphology and size of the nanocrystals are uniform and the nanocrystals are good dispersed in

solution. After coating β -UCNCs with SiO₂ (Fig.2b), amorphous TiO₂ (Fig.2c), and TiO₂ nanocrystals (Fig.2d and 2e), it can be clearly seen that the surface structure is changed remarkably. In Fig. 2b, it is clear that the surface of β -UCNCs @SiO₂ is smooth and the average thickness of SiO₂ is about 24nm. When TiO₂ is introduced onto the surface of β -UCNCs @SiO₂ (Fig. 2c, 2d and 2e), the double-shell structure of SiO₂ and TiO₂ can be observed. The outer TiO₂ shell is composed of a layer amorphous TiO₂ before annealing (Fig. 2c), and a large amount of tiny nanoparticles of anatase TiO₂ after hydrothermally annealing at 180° C for 24 h (Fig. 2d and 2e). These results are similar to our previous study and literature.^{29,40} These small sized TiO₂ nanoparticles dispersed around the surface of β -UCNCs@SiO₂ will result in a large specific surface area which can enhance the contact with contaminants for efficient photocatalytic degradation.²⁹ As shown in Fig. 2d and 2e, the morphology of β -UCNCs@SiO₂@TiO₂ and β -UCNCs@SiO₂@TiO₂:Mo is similar, indicating the Mo-doping has no influence on the morphology features. The HRTEM images of β -UCNCs (Fig. 2a, inset) and TiO₂ (Fig. 2e, inset) reveal highly crystalline natures of the as-prepared products. The interplanar distances between adjacent lattice fringes correspond to the crystal planes of the nanocrystals,^{40,41} good agreeing with the XRD detected results.

The composition of β -UCNCs@SiO₂@TiO₂:Mo was characterized by EDX analysis. As shown in Fig. 2f, almost all of the elements including Na, Lu, F, Gd, Yb, Tm, Ti, Mo, Si and O were detected, further confirmed the formation of the nanocomposite photocatalyst. The weight and atomic percentages of the elements in the composition were extracted from the EDX data. The determined weight and atomic ratios of Si/Ti/Lu are 2.17: 1.26 : 1 and 13: 5: 1, respectively.

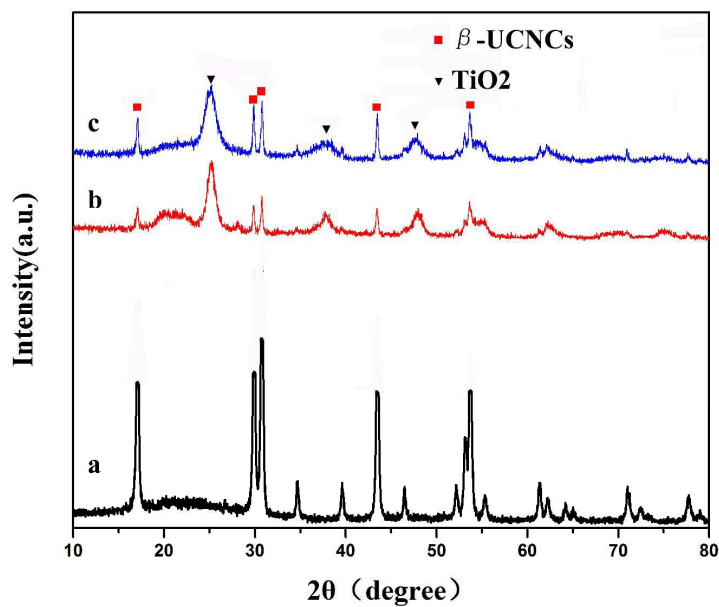


Fig. 1 XRD patterns of β -UCNCs (a), β -UCNCs@ SiO_2 @ TiO_2 (b) and β -UCNCs@ TiO_2 :Mo(c)

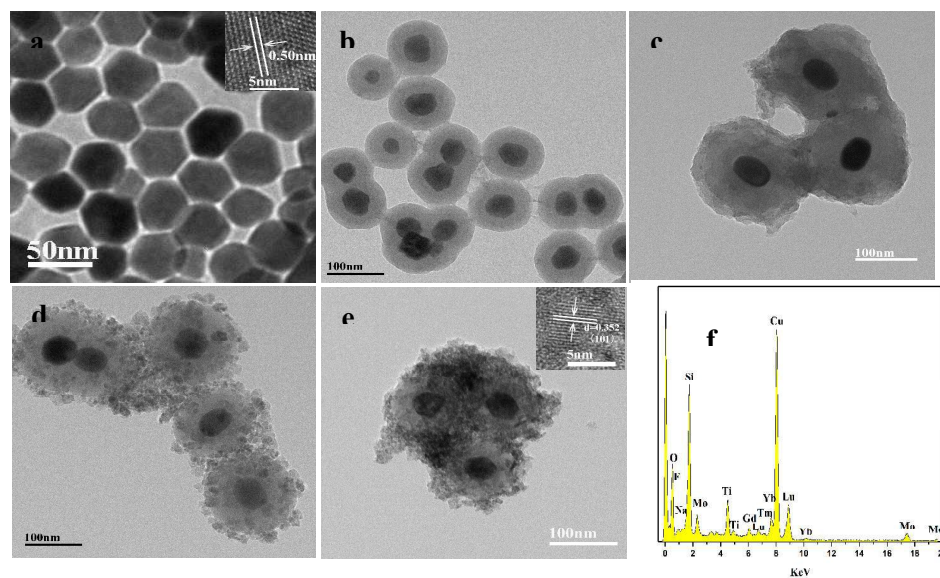


Fig. 2 TEM images of β -UCNCs(a), β -UCNCs@ SiO_2 (b), β -UCNCs@ SiO_2 @amorphous TiO_2 (c), β -UCNCs@ SiO_2 @ TiO_2 (d), and β -UCNCs@ SiO_2 @ TiO_2 :Mo(e). HRTEM images of β -UCNCs (1a, inset) and TiO_2 (2e, inset). EDX spectrum of β -UCNCs@ SiO_2 @ TiO_2 : Mo (f)

3.2. UV–vis absorption spectra analysis

UV–vis absorption spectra of β -UCNCs nanocrystal, β -UCNCs@SiO₂@TiO₂ nanocomposite, β -UCNCs@SiO₂@TiO₂:Mo nanocomposite and P25 are shown in Fig. 3. Except NaLuF₄:Gd,Yb,Tm, all the products have sharp peaks emerging at ~400 nm corresponding to the band-gap absorption of TiO₂.²⁹ Based on these UV-visible spectra, it can be speculated that the UV photos generated from the upconversion process of β -UCNCs can be absorbed by the anatase TiO₂ *via* an energy transfer. In comparison to P25 and β -UCNCs@SiO₂@TiO₂, there is an obvious red shift of absorption edge for β -UCNCs@SiO₂@TiO₂:Mo. This indicates that the narrowing of the band gap of TiO₂ occurs with the Mo-doping in TiO₂.^{36,37} For Mo⁶⁺-doped TiO₂, the incorporation of Mo⁶⁺ ions into TiO₂ lattice usually results in a formation of oxygen vacancies.³⁴ The charge compensation is achieved mainly by the ionized vacancies especially doubly ionized oxygen vacancies.³⁴ According to the energy band structure of TiO₂, the optical absorption in the UV range is mainly attributed to the electronic transitions from the valence band of O_{2p} to conduction band of Ti_{3d} (O_{2p} → Ti_{3d}). The optical absorption in the visible regions results mainly from sub-band transitions closely related to the ionized oxygen vacancies.³⁶ As a result of the extended photo responding range, a more efficient utilization of solar light could be achieved. It is also worth to notice that for β -UCNCs@SiO₂@TiO₂:Mo the light absorption in both UV and visible regions are greatly increased. The effective red shift of absorption edge and the evidently increased light absorption in UV-Visible region are significant benefit to the improvement of photocatalytic activity of the TiO₂-based photocatalyst.

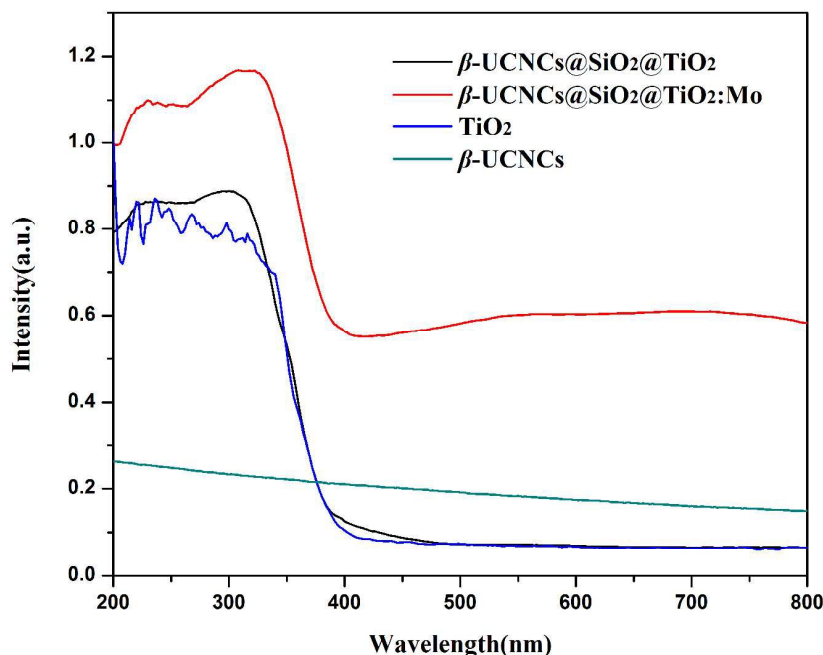


Fig. 3 UV-vis absorbance spectra of the products

3.3. Upconversion luminescence properties of the nanocomposite

The upconversion luminescence properties of the as-prepared products were investigated. As shown in Fig. 4, Under a 980 nm laser excitation, β -UCNCs emits UV and visible lights, where UV emission peaks centered at 361 nm is attributed to the transitions of Tm^{3+} ions: $^1\text{D}_2 \rightarrow ^3\text{H}_6$.^{29,42} The visible emission peaks at 450 nm, 476 nm, 645 nm and 697 nm are assigned to $^1\text{D}_2 \rightarrow ^3\text{H}_4$, $^1\text{G}_4 \rightarrow ^3\text{H}_6$, $^1\text{G}_4 \rightarrow ^3\text{F}_4$ and $^3\text{F}_3 \rightarrow ^3\text{H}_6$ transitions of Tm^{3+} ions,^{42,43} respectively. In order to evaluate the efficiency of the upconversion, the absolute UCL quantum yield of the β -UCNCs was measured to be $1.02 \pm 0.2\%$. It is reasonably high to fabricate effective upconversion photocatalyst for practical application.

The luminescence intensity of β -UCNCs@SiO₂ decreases a little compared to that of pure β -UCNCs. However, the coated SiO₂ shell with hydrophilic property can improve the dispersity of the catalyst in aqueous solutions so as to increase the contact between the pollutants and

as-prepared photocatalyst.⁴⁴ Furthermore, this SiO₂ layer will also prevent the electron trapping caused by surface defects and ligands of bare β -UCNCs,⁴⁵ and prevent the upconversion nanoparticles from photocatalysis induced corrosion to prolong its lifetime.⁴⁰ After further TiO₂ coating, the luminescence intensity decreases significantly compared to the β -UCNCs@SiO₂. The lights in UV region emitted by UCNCs are nearly disappeared, which can be attributed the absorbance of TiO₂ shell.²⁸ The lights in visible region for β -UCNCs@SiO₂@TiO₂ are also decreased, which can be assigned to the shielding effect of TiO₂ shell.⁴⁶ The emissions both in UV and visible regions for β -UCNCs@SiO₂@TiO₂:Mo are tremendously decreased and almost disappeared. As shown in Fig. 3, the emission bands of the UCNCs are all in the absorption range of the Mo ions-doped TiO₂. Since all of the emissions can be absorbed by TiO₂, meaning the energy transfer processes are efficient, it will be more beneficial to the photocatalysis.

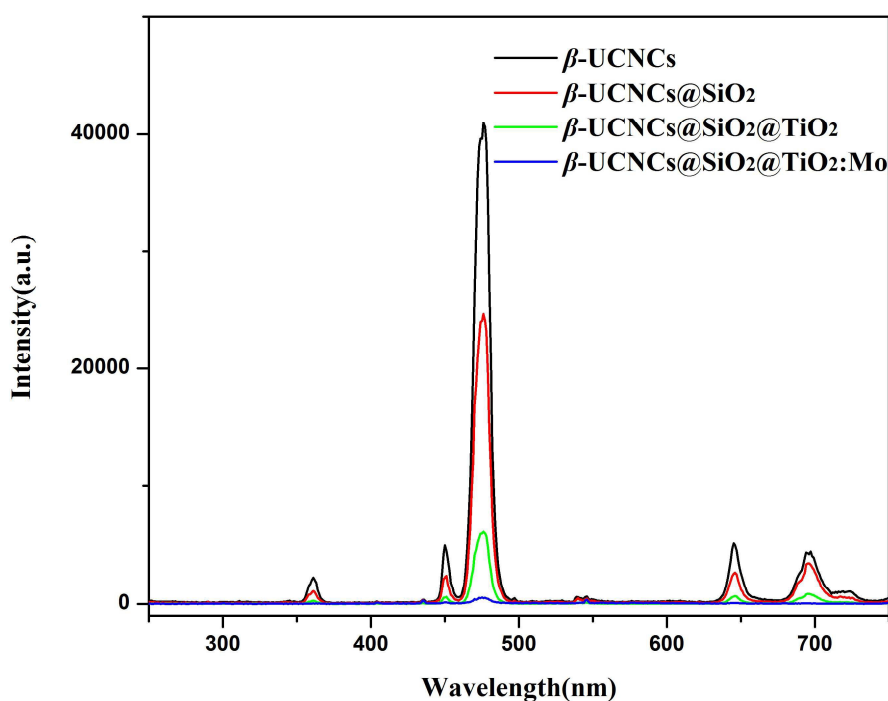


Fig. 4 Upconversion luminescent spectra of the prepared products under 980nm excitation

3.4. Photocatalytic measurements

Upon irradiation for a designated time, 1 mL RhB aqueous solution was taken out and diluted with 3ml deionized water for absorbance measurement. Fig. 5 shows the absorbance spectra of RhB catalyzed by the nanocomposite at different irradiation times. The absorption intensity of RhB at 554 nm decreases gradually with the increase in the irradiation time, indicating the degradation of RhB upon the simulated solar light irradiation.

The photocatalytic efficiency of the β -UCNCs@SiO₂@TiO₂:Mo nanocomposite photocatalyst can be evaluated through calculating the time-dependent degradation ratio of dye with contrast in blank, P25, TiO₂, β -UCNCs and β -UCNCs@SiO₂@TiO₂. Fig. 6 shows the time profile of C/C_0 under simulated solar light irradiation, where C is the concentration of RhB at the irradiation time and C_0 is the concentration of adsorption equilibrium with the photocatalysts before irradiation.

It can be seen from Fig. 6, the photocatalytic activity of β -UCNCs@SiO₂@TiO₂:Mo is remarkable higher than that of controls. The blank test confirms that RhB is quite stable. When catalyst is absent, no obvious change of RhB concentration is observed after irradiation for 210min. The similar result is observed for using pure β -UCNCs as catalyst, indicating β -UCNCs exhibits no catalytic activity. The RhB is almost completely degraded (99.44%) in the present of β -UCNCs @SiO₂@TiO₂:Mo after exposing under Xe lamp for 210min, whereas the degradation ratios of P25, TiO₂, β -UCNCs-TiO₂ physical mixture and NaLuF₄: Gd, Yb, Tm@SiO₂@TiO₂ are 30%, 25%, 55% and 82%, respectively. The photocatalytic activity of β -UCNCs @SiO₂@TiO₂:Mo is higher than β -UCNCs@SiO₂@TiO₂ that can be assigned to the function of Mo-doping which can narrow the band gap of TiO₂, extend photo responding range, and raise the light absorption in both UV and visible regions.³⁶ The photocatalytic activities of β -UCNCs@SiO₂@TiO₂:Mo and

β -UCNCs@SiO₂@TiO₂ are higher than β -UCNCs-TiO₂ physical mixture, which can be ascribed to the difference in their energy transfer efficiencies. There are no contact interfaces between UCNCs and TiO₂ particles in the physical mixture, thus the energy transfer efficiency is lower than that of the nanocomposites.^{27,29} In compared with commercial P25 which is well-known as benchmark catalyst, and pure TiO₂, the photocatalytic activity of β -UCNCs@SiO₂@TiO₂:Mo nanocomposite is significant higher (~3.31 and 3.98 times), demonstrating that the as-prepared nanocomposite photocatalyst can significant improve the photocatalytic activity of pure TiO₂.

According to the plots of $-\ln(c/c_0)$ vs. time, the photocatalytic degradation of RhB catalyzed by the prepared samples fits a first-order reaction kinetics well, that is, $-\ln(C/C_0) = \kappa t$, where κ is the apparent rate constant. In our experiment, κ is found to be 1.97×10^{-2} , 0.87×10^{-2} and 1.52×10^{-3} min⁻¹ for β -UCNCs@SiO₂@TiO₂:Mo, β -UCNCs@SiO₂@TiO₂ and P25, respectively. The degradation rate of β -UCNCs @SiO₂@TiO₂:Mo nanocomposite is about 13 times higher than that of P25. The high rate constant of β -UCNCs@SiO₂@TiO₂:Mo further confirmed its high photocatalytic activity. It is worth to note that the photocatalytic efficiency of the as-prepared product is higher than our previous reports and literatures.^{26,28,29,47-49}

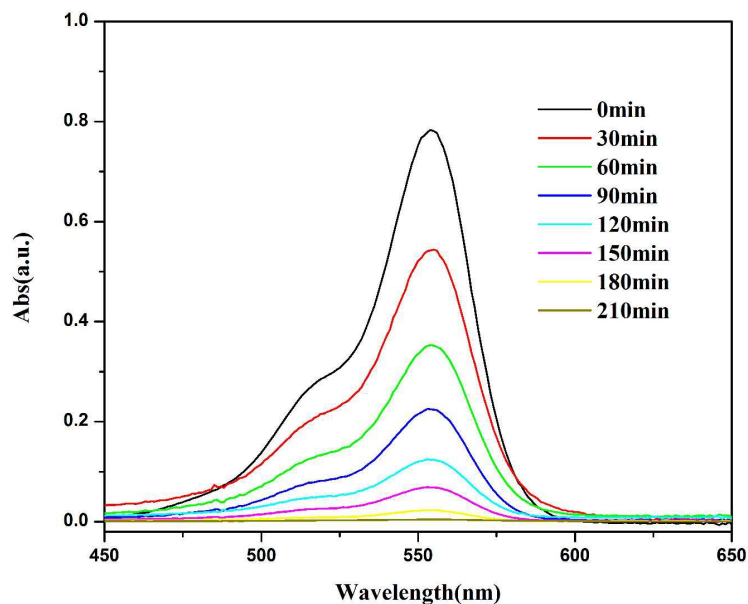


Fig. 5 Absorbance spectra of RhB catalyzed by the β -UCNCs @SiO₂@TiO₂:Mo nanocomposite at different irradiation times under simulated solar light irradiation

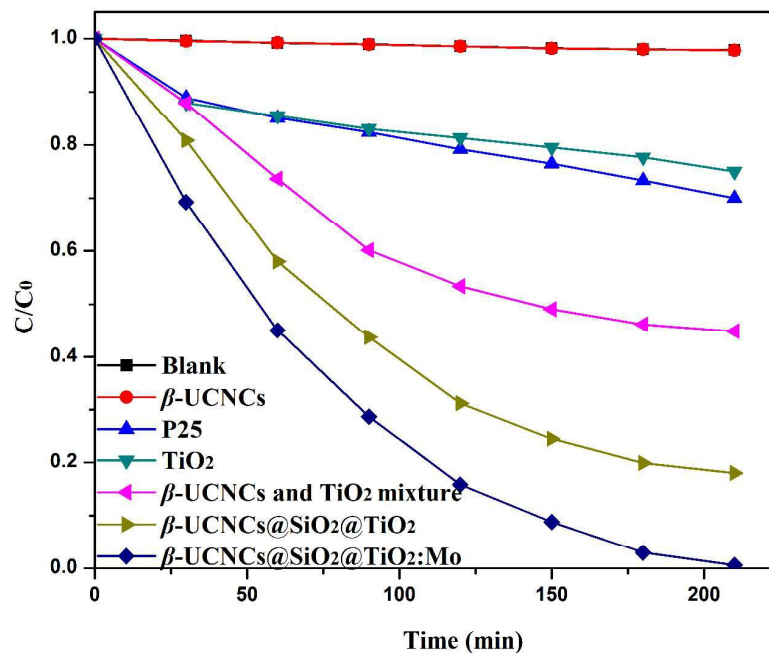


Fig. 6 Photocatalytic degradation of RhB under simulated solar light irradiation

In order to verify the advantage of the effect of the prepared upconversion photocatalyst, a test of photocatalytic degradation under NIR (980nm) irradiation was performed. The obtained results are shown in Fig.7. Similar to the results obtained under simulated solar irradiation, the RhB is almost completely degraded in the present of β -UCNCs @SiO₂@TiO₂:Mo after exposing under 980nm light for 210min, and it is much higher than that of control. These results demonstrate that the as-prepared photocatalyst of β -UCNCs@SiO₂@TiO₂:Mo also has high photocatalytic activity under NIR irradiation in comparison to the controls, further proving the advantage of the as-prepared product.

To investigate the durability of photocatalytic activity of the product under the simulated solar and NIR irradiations, we repeated the same photocatalytic degradation test of β -UCNCs@SiO₂@TiO₂:Mo for four cycles. As can be observed in Fig. 8, both the simulated solar and NIR-driven photocatalytic activities of the product are very stable.

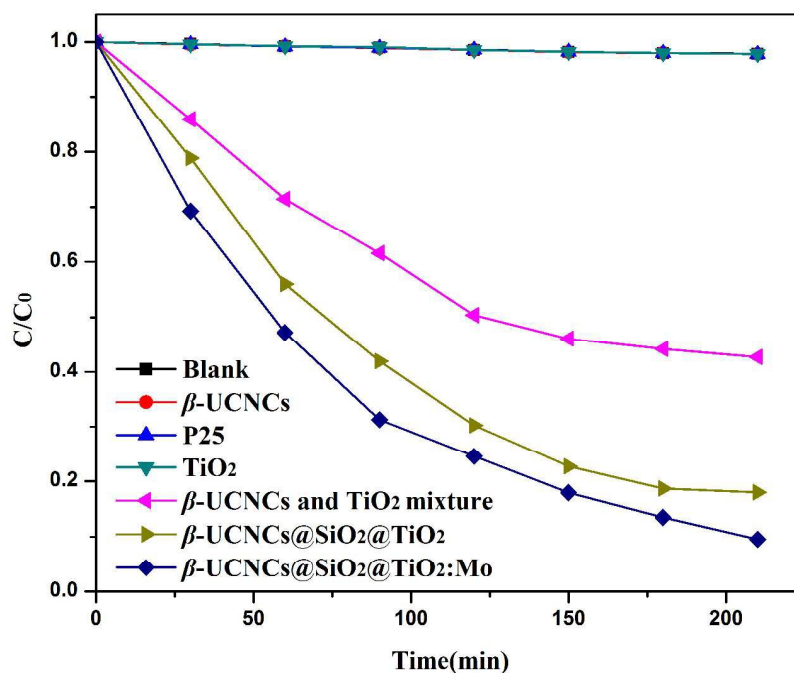


Fig. 7 Photocatalytic degradation of RhB under 980nm light irradiation

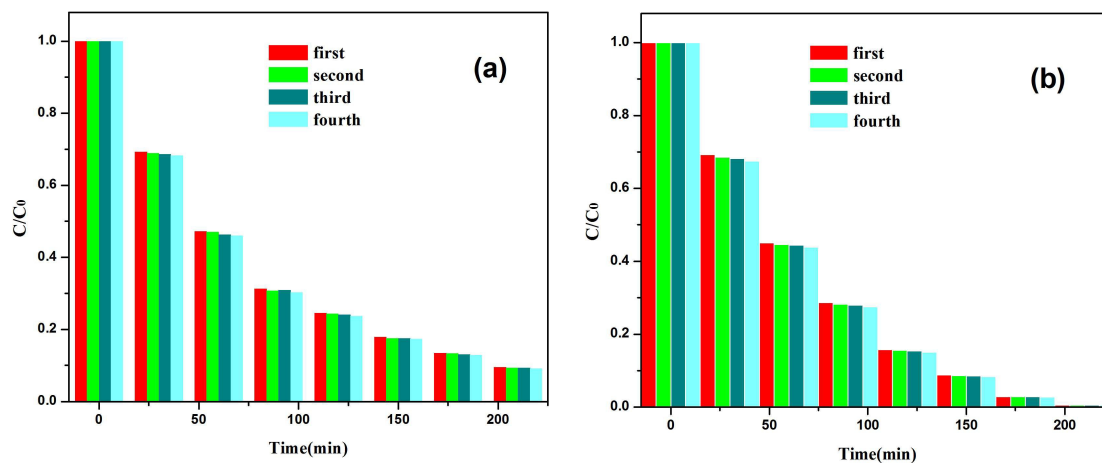


Fig. 8. Repeated photocatalytic activity measurements with the presence of β -UCNCs@SiO₂@TiO₂:Mo under the irradiations of 980nm light (a), and simulated solar light (b).

The high photocatalytic activity of the as-prepared photocatalyst β -UCNCs@SiO₂@TiO₂:Mo can be ascribed to two aspects. One is the function of the upconversion nanocrystal β -UCNCs and the other is the effect of Mo-doping. Under the simulated solar or NIR light irradiation, the

β -UCNCs can absorb the NIR region light and upconvert it into UV and visible lights which can be overall absorbed by modified TiO₂. More important, the high energetic UV photons absorbed by the TiO₂ can drive the TiO₂ to generate high energetic electrons and holes pairs.²⁹ These photoproduced electrons and holes pairs possessing high oxidation-reduction potentials and high oxidation-reduction abilities.²⁸ On the other hand, due to the narrowing band gap of TiO₂ caused by Mo-doping, the absorption of photons from solar-driven light illumination can be effectively enhanced, resulting in improving the photocatalytic efficiency.³⁶ Furthermore, Mo⁶⁺ ions replacing Ti⁴⁺ ions in the lattice act as electron traps to promote the charge separation and to reduce the recombination rate of the photogenerated carriers.⁵⁰

The photocatalysis and energy transfer processes are as following: the outer TiO₂ layer can quickly absorb the UV and visible light from solar lights, for its intrinsic property and its bandgap modification by Mo-doping. The high penetrability of the NIR from the solar light allows it to go further into the inner to excite the β -UCNCs emitting UV and visible lights, which are all in the modified-TiO₂ absorption range. Then the upconverted lights will pass through the transparent SiO₂ layer to excite the outer TiO₂ nanocrystals. After absorbing the solar and upconverted lights, the excited TiO₂ generates electron-hole pairs. These electron-hole pairs then migrate from inner region to the surfaces and act as catalytic centre. These electrons and holes can not only directly decompose the pollutant, but also degrade the pollutant indirectly through $\cdot\text{OH}$ and $\cdot\text{O}_2^-$ radicals that are produced from oxidizing H₂O and reducing O₂ molecules by the holes and electrons, respectively.²⁸

4. Conclusions

In summary, a novel double-shell-structured β -UCNCs@SiO₂@TiO₂:Mo nanocomposite photocatalyst was synthesized successfully. The designed structure gives effective energy transfer from UCNCs to TiO₂, and improves the light absorption in both UV and visible ranges. The photocatalytic activities of the products were evaluated through photocatalytic degradation dye of RhB under the simulated solar light and NIR irradiations. It was found that the photocatalytic activity of the nanocomposite photocatalyst has been substantially improved in comparison to the pure TiO₂ and P25. This work gives a new insight on significantly improving the photocatalytic activity of TiO₂ under solar light irradiation by employing proper UCNCs and doping transition metal ions simultaneously. The as-prepared nanocomposite photocatalyst exhibiting superior photocatalytic activity is potential to be used for environmental cleaning.

Acknowledgments

The authors acknowledge the National Natural Science Foundation of China (No. 21271126, 11025526), Program for Innovative Research Team in University (No. IRT 13078), and National 973 Program (No.2010CB933901).

Notes and References

- 1 L. M. Pastrana-Martínez, S. Morales-Torres, V. Likodimos, J. L. Figueiredo, J. L. Faria, P. Falaras and M. T. Adrian Silva, *Appl. Catal. B: Environ.*, 2012, **123**, 241.
- 2 R. Chalasani and S. Vasudevan, *Acs. Nano.*, 2013, **7**, 4093.
- 3 T. Fotiou, T. M. Triantis, T. Kaloudis and A. Hiskia, *J. Chem. Eng.*, 2015, **261**: 17.

- 4 M. G. Walter, E. L. Warren, J. R. McKone, W. S. Boettcher, Q. X. Mi, A. S. Elizabeth and N. S. Lewis, *Chem. Rev.*, 2010, **110**, 6446.
- 5 X. Yang, J. Qin, Y. Li, R. X. Zhang and H. Tang, *J. Hazard. Mater.*, 2013, **261**, 342.
- 6 X. Yang, J. Qin, Y. Jiang, R. Li, Y. Li and H. Tang, *Rsc. Adv.*, 2014, **4**, 18627.
- 7 H. Tang, D. Zhang and G. Tang, *Ceram. Int.*, 2013, **39**, 8633.
- 8 G. Tang, S. Liu, H. Tang, D. Zhang, C. S. Li and X. F. Yang, *Ceram. Int.*, 2013, **39**, 4969.
- 9 X. Zhang, Y. Sun, X. Cui and Z. Y. Jiang, *Int. J. Hydrogen. Energ.*, 2012, **37**, 1356.
- 10 Q. Zhang, W. Li and S. Liu, *Powder. Technol.*, 2011, **212**, 145.
- 11 J. Pascual, J. Camassel and H. Mathieu, *Phys. Rev. Lett.*, 1977, **39**, 1490.
- 12 K. Yang, Y. Dai and B. Huang, *J. Phys. Chem. C.*, 2007, **111**, 12086.
- 13 J. L. Gole, J. D. Stout, C. Burda, Y. B. Lou and X. B. Chen, *J. Phys. Chem. B.*, 2004, **108**, 1230.
- 14 G. Liu, Y. Zhao, C. Sun, F. Li, G. Q. Lu and H. M. Cheng, *Angew. Chem. Int. Ed.*, 2008, **47**, 4516.
- 15 K. T. Ranjit and B. Viswanathan, *J. Photoch. Photobio. A: Chem.*, 1997, **108**, 79.
- 16 Y. Huo, J. Zhu, J. Li, G. S. Li and H. X. Li, *J. Mol. Catal. A: Chem.*, 2007, **278**, 237.
- 17 Z. Liu, B. Guo, L. Hong and H. X. Jiang, *J. Phys. Chem. Solids.*, 2005, **66**, 161.
- 18 R. Asahi, T. Morikawa, T. Ohwaki, K. Aoki and Y. Taga, *Science*, 2001, **293**, 269.
- 19 M. Sathish, B. Viswanathan, R. P. Viswanath and S. G. Chinnakonda, *Chem. Mater.*, 2005, **17**, 6349.
- 20 S. Sakthivel and H. Kisch, *Angew. Chem. Int. Ed.*, 2003, **42**, 4908.
- 21 J. C. Yu, J. Yu, W. Ho, Z. T. Jiang and L. Z. Zhang, *Chem. Mater.*, 2002, **14**, 3808.

- 22 W. Fan, S. Jewell and Y. She, *Phys. Chem. Chem. Phys.*, 2013, **16**, 676.
- 23 J. Xu, W. Wang, S. Sun and L. Wang, *Appl. Catal. B: Environ.*, 2012, **111**, 126.
- 24 J. Wang, F. Wen, Z. Zhang, X. D. Zhang, Z. J. Pan, L. Zhang, L. Wang, L. Xu, P. L. Kang and P. Zhang, *J. Environ. Sci.*, 2005, **17**, 727.
- 25 G. Feng, S. Liu, Z. Xiu, Y. Zhang, J. X. Yu, Y. G. Chen, P. Wang and X. J. Yu, *J. Phys. Chem. C.*, 2008, **112**, 13692.
- 26 D. G. Yin, L. Zhang and K. L. Song, *J. Nanosci. Nanotechnol.*, 2014, **14**, 6077.
- 27 Y. Zhang and Z. Hong, *Nanoscale*, 2013, **5**: 8930.
- 28 Y. Tang, W. Di, X. Zhai, R. Y. Yang and W. P. Qin, *ACS Catal.*, 2013, **3**, 405.
- 29 C. C. Wang, K. L. Song, Y. Feng, D. G. Yin, J. Ouyang, B. Liu, X. Z. Cao, L. Zhang, Y. L. Han and M. H. Wu, *RSC Adv.*, 2014, **4**, 39118.
- 30 L. Ren, X. Qi, Y. Liu, Z. Y. Huang, X. L. Wei, J. Li, L. W. Yang and J. X. Zhong, *J. Mater. Chem.*, 2012, **22**, 11765.
- 31 D. G. Yin, C. C. Wang, J. Ouyang, X. Y. Zhang, Y. Feng, K. L. Song, B. Liu, X. Z. Cao, L. Zhang, H. Y. Lin and M. H. Wu, *ACS Appl. Mater. Inter.*, 2014, **6**, 18480.
- 32 F. Wang, Y. Han, C. S. Lin, Y. H. Lu, J. Wang, J. Xu, H. Chen, C. Zhang, M. H. Hong and X. G. Liu, *Nature*, 2010, **463**, 1061
- 33 Y. Q. Gai, J. B. Li and S. S. Li, *Phys. Rev. Lett.*, 2009, **102**, 036402.
- 34 L. G. Devi and B. N. Murthy, *Catal. Lett.*, 2008, **125**, 320.
- 35 X. Yu, C. Li, Y. Ling, T. Tang, Q. Wu and J. Kong, *J. Alloy. Compd.*, 2010, **507**, 33.
- 36 D. G. Yin, X. Z. Cao, L. Zhang, J. X. Tang, W. F. Huang, Y. L. Han and M. H. Wu, *Dalton. T.*, 2015, **44**, 11147.

- 37 M.S. Jeon, W.S. Yoon, J. Hyunku, T.K. Lee and H.J. Lee, *Appl. Surf. Sci.*, 2000, **165**, 209.
- 38 N. Niu, P. P. Yang, F. He, X. Zhang, S. L. Gai, C. X. Li and J. Lin, *J. Mater. Chem.*, 2012, **22**, 10889.
- 39 D. H. Chen, F. Z. Huang, Y. B. Cheng and R. A. Caruso, *Adv. Mater.*, 2009, **21**, 2206.
- 40 W. Wang, W. J. Huang, Y. R. Ni, C. H. Lu and Z. Z. Xu, *Acs. Appl. Mater. Inter.*, 2013, **6**, 340.
- 41 J. Ouyang, D. G. Yin, X. Z. Cao, C. C. Wang, K. L. Song, B. Liu, L. Zhang, Y. L. Han and M. H. Wu, *Dalton. T.*, 2014, **43**, 14001.
- 42 N. Liu, W. P. Qin, G. S. Qin, T. Jiang and D. Zhao, *Chem. Commun.*, 2011, **47**, 7671.
- 43 S. H. Tang, J. N. Wang, C. X. Yang, L. X. Dong, D. L. Kong and X. P. Yan, *Nanoscale*, 2014, **6**, 8037.
- 44 H. Y. Xing, W. B. Bu, S. J. Zhang, X. P. Zheng, M. Li, F. Chen, Q. J. He, L. P. Zhou, W. J. Peng, Y. Q. Hua and J. L. Shi, *Biomaterials*, 2012, **33**, 1079.
- 45 L. L. Liang, Y. M. Liu, C. H. Bu, K. M. Guo, W. W. Sun, N. Huang, T. Peng, B. Sebo, M. M. Pan, W. Liu, S. S. Guo and X. Z. Zhao, *Adv. Mater.*, 2013, **25**, 2174.
- 46 W. P. Qin, D. S. Zhang, D. Zhao, L. L. Wang and K. Z. Zheng, *Chem. Commun.*, 2010, **46**, 2304.
- 47 Y. Y. Lv, L. S. Yu, H. Y. Huang, H. L. Liu and Y. Y. Feng, *J. Alloy. Compd.*, 2009, **488**, 314.
- 48 J. K. Zhou, M. Takeuchi, X. S. Zhao, A. K. Ray and M. Anpo, *Catal. Lett.*, 2006, **106**, 67.
- 49 D. G. Yin, Le. Zhang, B. H. Liu and M. H. Wu, *J. Nanosci. Nanotechno.*, 2012, **12**, 937.
- 50 M. E. Simonsen, Z. S. Li and E. G. Søgaard, *Appl. Surf. Sci.*, 2009, **255**, 8054.